examined sensitivity to the acetylcholinesterase inhibitor aldicarb. Aldicarb causes paralysis of body movement resulting from the accumulation of acetylcholine at the neuromuscular junction (*18*). Mutations that reduce synaptic transmission cause resistance to aldicarb (*18*). In contrast, mutations that stimulate synaptic transmission cause hypersensitivity to aldicarb-mediated paralysis (*19*). Trimethadione treatment of wild-type animals caused hypersensitivity to aldicarb-mediated paralysis (Fig. 3E). The control drug, succinimide, did not cause hyperactive motility or aldicarb hypersensitivity (*3*). These results indicate the anticonvulsants stimulate synaptic transmission in the neuromuscular system that controls body movement.

Ethosuximide and trimethadione effectively treat absence seizures in humans by regulating neural activity. A likely target of ethosuximide is T-type calcium channels, although it is possible that these compounds act on multiple targets (*20–22*). These anticonvulsants also affected neural activity in nematodes, and the anticonvulsant and the life-span extension effects of the compounds may act through similar mechanisms. The findings presented here are consistent with the model that the effect on neural activity causes the life-span extension, although they do not exclude the possibility that the drugs affect neural activity and aging by different mechanisms. Furthermore, the interactions with the insulin-signaling mutants suggest the intriguing possibility that neural activity regulates aging by both *daf-16*–dependent and *daf-16*–independent mechanisms.

References and Notes

1. L. Guarente, C. Kenyon, *Nature* **408**, 255 (2000).
2. Materials and methods are available as supporting material on *Science* Online.
3. S. Hughes, K. Evason, data not shown.
4. B. G. Katzung, Ed., *Basic and Clinical Pharmacology* (Appleton and Lange, Upper Saddle River, NJ, ed. 7, 1998).
5. R. H. Levy, R. H. Mattson, B. S. Meldrum, E. Perucca, Eds., *Antiepileptic drugs* (Lippincott, Williams and Wilkins, Philadelphia, ed. 5, 2002).
6. P. A. Reddy *et al.*, *J. Med. Chem.* **39**, 1898 (1996).
7. C. Huang, C. Xiong, K. Kornfeld, *Proc. Natl. Acad. Sci. U.S.A.* **101**, 8084 (2004).
8. D. Gems, D. L. Riddle, *Genetics* **154**, 1597 (2000).
9. D. A. Garsin *et al.*, *Science* **300**, 1921 (2003).
10. J. P. McKay, D. M. Raizen, A. Gottschalk, W. R. Schafer, L. Avery, *Genetics* **166**, 161 (2004).
11. B. Lakowski, S. Hekimi, *Proc. Natl. Acad. Sci. U.S.A.* **95**, 13091 (1998).
12. C. Kenyon, J. Chang, E. Gensch, A. Rudner, R. Tabtiang, *Nature* **366**, 461 (1993).
13. D. Gems, S. Pletcher, L. Partridge, *Aging Cell* **1**, 1 (2002).
14. J. Apfeld, C. Kenyon, *Nature* **402**, 804 (1999).
15. M. Ailion, T. Inoue, C. I. Weaver, R. W. Holdcraft, J. H. Thomas, *Proc. Natl. Acad. Sci. U.S.A.* **96**, 7394 (1999).
16. D. L. Riddle, Ed., *C. elegans II, Cold Spring Harbor Monogr. Ser. 33* (Cold Spring Harbor Laboratory Press, Plainview, NY, 1997).
17. C. Trent, N. Tsuing, H. R. Horvitz, *Genetics* **104**, 619 (1983).
18. K. G. Miller *et al.*, *Proc. Natl. Acad. Sci. U.S.A.* **93**, 12593 (1996).
19. K. G. Miller, M. D. Emerson, J. B. Rand, *Neuron* **24**, 323 (1999).
20. D. A. Coulter, J. R. Huguenard, D. A. Prince, *Ann. Neurol.* **25**, 582 (1989).
21. J. C. Gomora, A. N. Daud, M. Weiergraber, E. Perez-Reyes, *Mol. Pharmacol.* **60**, 1121 (2001).
22. N. Leresche *et al.*, *J. Neurosci.* **18**, 4842 (1998).

23. Strains were provided by the *Caenorhabditis* Genetics Center, which is funded by the NIH National Center for Research Resources. We thank M. Nonet for helpful suggestions and *aex-3* mutants, S. Hughes for experimental assistance, and D. Redmond for assistance with graphics. Support was provided by the Washington University Alzheimer's Disease Research Center (grant no. P50 AG05681) and the Longer Life Foundation, a Reinsurance Group of America, Inc. (RGA)/Washington University Partnership (grant no. 1999-001). C.H. was supported by a Predoctoral Fellowship from the Howard Hughes Medical Institute. K.K. is a scholar of the Leukemia and Lymphoma Society.

Supporting Online Material
www.sciencemag.org/cgi/content/full/307/5707/258/DC1
Materials and Methods
Fig. S1
References

16 September 2004; accepted 16 November 2004
10.1126/science.1105299

Self-Propagating, Molecular-Level Polymorphism in Alzheimer's β-Amyloid Fibrils

Aneta T. Petkova,[1] Richard D. Leapman,[2] Zhihong Guo,[3] Wai-Ming Yau,[1] Mark P. Mattson,[3] Robert Tycko[1]*

Amyloid fibrils commonly exhibit multiple distinct morphologies in electron microscope and atomic force microscope images, often within a single image field. By using electron microscopy and solid-state nuclear magnetic resonance measurements on fibrils formed by the 40-residue β-amyloid peptide of Alzheimer's disease ($A\beta_{1-40}$), we show that different fibril morphologies have different underlying molecular structures, that the predominant structure can be controlled by subtle variations in fibril growth conditions, and that both morphology and molecular structure are self-propagating when fibrils grow from preformed seeds. Different $A\beta_{1-40}$ fibril morphologies also have significantly different toxicities in neuronal cell cultures. These results have implications for the mechanism of amyloid formation, the phenomenon of strains in prion diseases, the role of amyloid fibrils in amyloid diseases, and the development of amyloid-based nanomaterials.

Amyloid fibrils are self-assembled filamentous aggregates formed by peptides and proteins with diverse amino acid sequences (*1*). Current interest in amyloid fibrils arises from their involvement in Alzheimer's disease (AD), type 2 diabetes, prion diseases, and other protein misfolding disorders (*2*) and from basic questions about the interactions that stabilize amyloid structures and the mechanisms by which they form (*3*). Recent experiments additionally suggest that amyloid structures may be a basis for one-dimensional nanomaterials with possible technological applications (*4*, *5*).

In transmission electron microscope (TEM) and atomic force microscope (AFM) images, amyloid fibrils commonly exhibit multiple distinct morphologies, often described as twisted or parallel assemblies of finer protofilaments (*6–8*). Two explanations for amyloid polymorphism are possible: (i) distinct morphologies result from distinct modes of lateral association of protofilaments without significant variations in molecular structure (*7*) or (ii) distinct morphologies result from significant variations in molecular structure at the protofilament level. Here, we report electron microscopy and solid-state nuclear magnetic resonance (NMR) data on amyloid fibrils formed by the 40-residue β-amyloid peptide associated with AD ($A\beta_{1-40}$) that support the second possibility and reveal specific molecular-level structural differences between different fibril morphologies. The predominant morphology and molecular structure are sensitive to subtle differences in fibril growth conditions in de novo preparations (at fixed pH, temperature, buffer composition, and peptide concentration), but both morphology and molecular structure are self-propagating in seeded preparations. Different $A\beta_{1-40}$ fibril morphologies also exhibit significantly different toxicities in neuronal cell cultures.

[1]Laboratory of Chemical Physics, National Institute of Diabetes and Digestive and Kidney Diseases, National Institutes of Health (NIH), Bethesda, MD 20892–0520, USA. [2]Division of Bioengineering and Physical Science, Office of Research Services, NIH, Bethesda, MD 20892–5766, USA. [3]Laboratory of Neurosciences, National Institute of Aging, NIH, Baltimore, MD 21224–6825, USA.

*To whom correspondence should be addressed. E-mail: rt46d@nih.gov

Reproduced with permission of the copyright owner. Further reproduction prohibited without permission.

Amyloid fibrils were prepared from the human $A\beta_{1-40}$ peptide (sequence NH_2-DAEFRHDSGY EVHHQKLVFF AEDVGSNKGA IIGLMVGGVV-COOH) (*9*, *10*). Parent fibrils were grown by incubation of identical fresh $A\beta_{1-40}$ solutions for periods of 21 to 68 days either in vertical dialysis tubes in an unstirred bath of buffer or in horizontal polypropylene tubes with gentle circular agitation (Red Rotor orbital mixer, Hoefer Scientific Instruments, San Francisco, CA), producing quiescent and agitated parent fibrils, respectively. Daughter fibrils were grown under dialysis conditions by seeding fresh solutions with sonicated fragments (9.1% of total $A\beta_{1-40}$) of either quiescent or agitated parents. Daughter fibrils were used as seeds for granddaughter fibrils, also grown under dialysis conditions. Daughter and granddaughter fibrils were grown for 3 to 8 days.

TEM images of negatively stained $A\beta_{1-40}$ fibrils are shown in Fig. 1 (*9*). The predominant morphology for quiescent parents is a fibril with a periodically modulated width (50- to 200-nm period and 12- ± 1-nm maximum width), commonly ascribed to a periodic twist (*6*–*8*). The predominant morphology for agitated parents is a filament with no resolvable twist (5.5- ± 0.5-nm width) but with a pronounced tendency to associate laterally into dimers or multimers. Morphological differences are preserved in TEM images of sonicated seeds and are transmitted to daughter and granddaughter fibrils, even though all daughter and granddaughter fibrils were grown under identical dialysis conditions. AFM images show similar morphological differences (fig. S1).

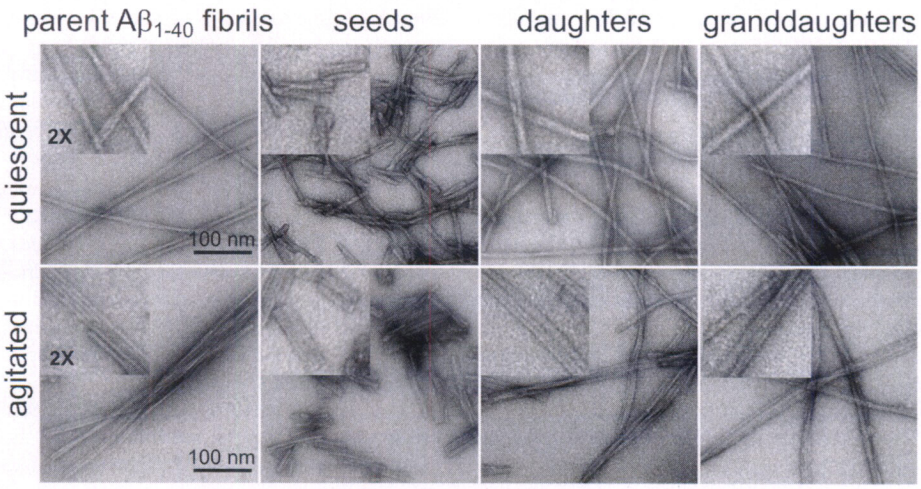

Fig. 1. TEM images of amyloid fibrils formed by the $A\beta_{1-40}$ peptide, negatively stained with uranyl acetate. Parent fibrils were prepared by incubation of $A\beta_{1-40}$ solutions either under quiescent dialysis conditions or in a closed polypropylene tube with gentle agitation. Daughter and granddaughter fibrils were grown under dialysis from solutions that were seeded with sonicated fragments of parent and daughter fibrils, respectively.

Molecular and supramolecular structures of amyloid fibrils can be probed by various solid-state NMR techniques (*3*, *11*–*16*). Figure 2 shows two-dimensional (2D) solid-state ^{13}C NMR spectra of parent, daughter, and granddaughter fibrils with uniform labeling of F20, D23, V24, K28, G29, A30, and I31 (*9*). The patterns of strong one-bond cross peaks in these spectra are determined by isotropic ^{13}C chemical shifts, which are sensitive to local structural and conformational environment (*13*, *17*, *18*). Remarkably, the 2D spectra of quiescent and agitated parent fibrils show pronounced differences in cross-peak patterns that are transmitted to the daughter and granddaughter fibrils. Thus, the morphological differences in Fig. 1 correlate with underlying differences in structure at the molecular level. The ^{13}C chemical shift differences are greater than 1.5 parts per million (ppm) at multiple backbone and side-chain

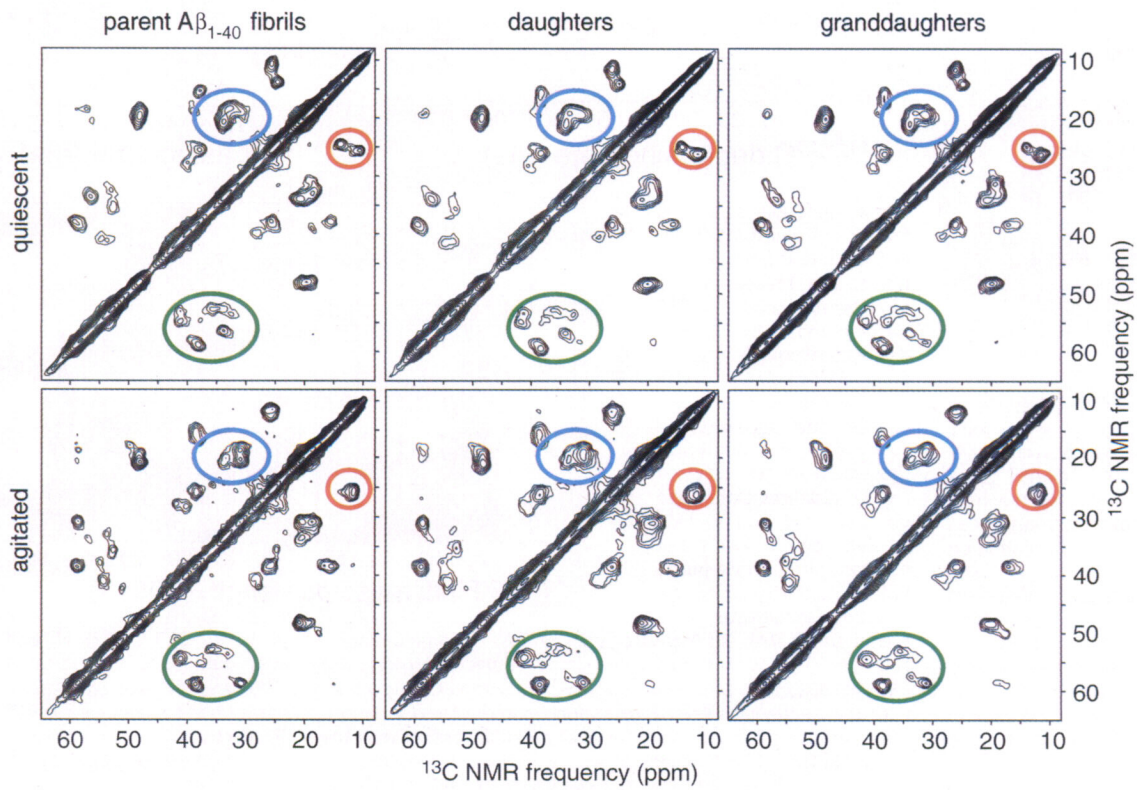

Fig. 2. Two-dimensional solid-state ^{13}C NMR spectra of $A\beta_{1-40}$ fibrils, prepared with ^{13}C labeling of all carbon sites in amino acid residues F20, D23, V24, K28, G29, A30, and I31. Spectra were recorded under magic angle spinning. Regions enclosed by ellipses contain $C_{\gamma 1}/C_{\delta}$ cross peaks of I31 (red), C_{β}/C_{γ} cross peaks of V24 (blue), and C_{α}/C_{β} cross peaks of F20, D23, V24, K28, and I31 (green).

Reproduced with permission of the copyright owner. Further reproduction prohibited without permission.

sites (tables S1 and S2) and are independent of the protocol used to prepare $A\beta_{1-40}$ solutions for parent fibril growth (fig. S2).

The propensities for lateral association exhibited by quiescent and agitated fibrils suggest that different amino acid side chains are exposed on the fibril surfaces, possibly leading to different biological activities. Figure 3 shows the results of measurements of $A\beta_{1-40}$ fibril toxicity in cultures of primary rat embryonic hippocampal neurons (*9*). Both quiescent and agitated fibrils are neurotoxic at $A\beta_{1-40}$ concentrations of 10 μM and above, but the toxicity of quiescent fibrils is significantly higher than that of agitated fibrils. Toxicity measurements on nonfibrillar $A\beta_{1-40}$ aggregates, which form in unseeded solutions at early stages of incubation, show no significant difference between quiescent and agitated conditions (fig. S3).

Some specific structural features of quiescent and agitated $A\beta_{1-40}$ fibrils are indicated in Fig. 4. All amyloid structures contain the cross-β motif, i.e., β sheets extending over the length of the fibril, with β strands roughly perpendicular to and interstrand hydrogen bonds roughly parallel to the long fibril axis (*1*, *3*). Intermolecular ^{13}C-^{13}C nuclear magnetic dipole-dipole couplings (Fig. 4A) indicate intermolecular distances of 0.55 ± 0.05 nm at V12, V39, and A30, implying in-register, parallel β sheets for both morphologies as reported previously for $A\beta_{10-35}$ and $A\beta_{1-40}$ fibrils prepared with different protocols (*12*, *14*, *15*, *19*). The ^{15}N-^{13}C dipole-dipole couplings (Fig. 4B) indicate a 0.32 ± 0.02-nm distance between side-chain C_γ carbons of D23 residues and side-chain N_ζ nitrogens of K28 residues in agitated $A\beta_{1-40}$ fibrils, consistent with salt bridges between oppositely charged D23 and K28 side chains. Weaker D23-K28 couplings are observed in quiescent fibrils, consistent with longer average C_γ-N_ζ distances. Dipole-dipole couplings between side-chain C_δ carbons of E22 residues and side-chain N_ζ nitrogens of K16 residues are observed in quiescent fibrils, possibly indicating partial occupation of an intermolecular K16-E22 salt bridge, but are absent in agitated fibrils. Histograms of fibril mass-per-length (MPL) (Fig. 4C) obtained from scanning transmission electron microscope (STEM) images (*9*) show mode values of 21.4 kD/nm for agitated fibrils [similar to earlier $A\beta_{1-40}$ and $A\beta_{1-42}$ fibril STEM data (*6*, *15*)] and 30.3 kD/nm for quiescent fibrils. Given the 0.47- to 0.48-nm spacing between peptide chains in an ideal cross-β structure, the MPL of one layer of $A\beta_{1-40}$ molecules (4.3 kD mass) would be 9.1 kD/nm. Figure 4C suggests that the protofilament (defined here as the experimentally detected structure with minimal MPL) contains two molecular layers in agitated $A\beta_{1-40}$ fibrils and three molecular layers in quiescent $A\beta_{1-40}$ fibrils. Deviations from precise integer multiples of 9.1 kD/nm may arise from a nonzero angle θ between the interstrand hydrogen bonding direction and the long fibril axis, which would increase the MPL values by 1/cos θ.

Established correlations between ^{13}C NMR chemical shifts and secondary structure (*13*, *17*) and predictions of backbone φ and ψ torsion angles from the TALOS program (*18*) suggest that the β strand segments in quiescent $A\beta_{1-40}$ fibrils include residues 10 to 14, 16 to 22, 30 to 32, and 34 to 36, whereas those in agitated $A\beta_{1-40}$ fibrils include residues 10 to 22, 30 to 32, and 34 to 36 (tables S1 and S2). Figure 4A shows that V12 and V39 participate in the parallel, hydrogen-bonded structure in both polymorphs. The ^{13}C chemical shifts for Q15, D23, G25, and G33 in quiescent fibrils and for D23, G25, and G33 in agitated fibrils suggest non-β strand conformations at these residues. The ^{13}C NMR linewidths (fig. S4) indicate structurally disordered N-terminal segments in both morphologies, as previously suggested (*13*, *14*, *19*–*21*). Linewidths for most CO, C_α, and C_β sites in residues 12 to 39 of quiescent fibrils and residues 10 to 39 of agitated fibrils are 2.5 ppm or less, indicating overall structural order (*13*).

Data for agitated $A\beta_{1-40}$ fibrils are largely consistent with our recent model for the

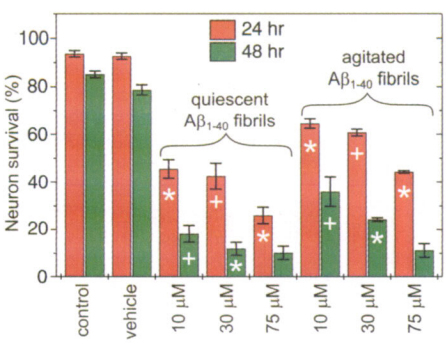

Fig. 3. Toxicity of $A\beta_{1-40}$ fibrils in cultures of primary embryonic rat hippocampal neurons, assayed by counting viable neurons after 24-hour and 48-hour exposures to $A\beta_{1-40}$ at indicated concentrations in neurobasal medium. Error bars indicate standard errors on mean survival values (four culture dishes per condition and 35 to 145 neurons monitored per dish). Control is neurobasal medium alone. Vehicle is supernatant after centrifugation of $A\beta_{1-40}$ fibril solution, added to neurobasal medium in volume equal to that for 30 μM conditions. The asterisks and plus symbols indicate conditions where toxicity differences between quiescent and agitated fibrils are statistically significant (analysis of variance test, $P < 0.01$ and $P < 0.05$, respectively).

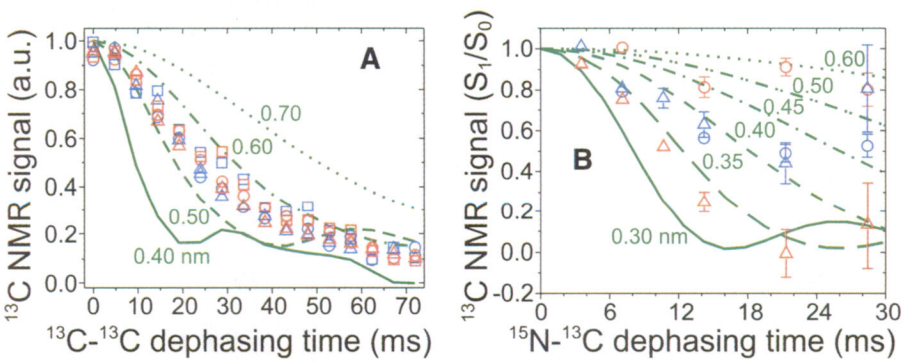

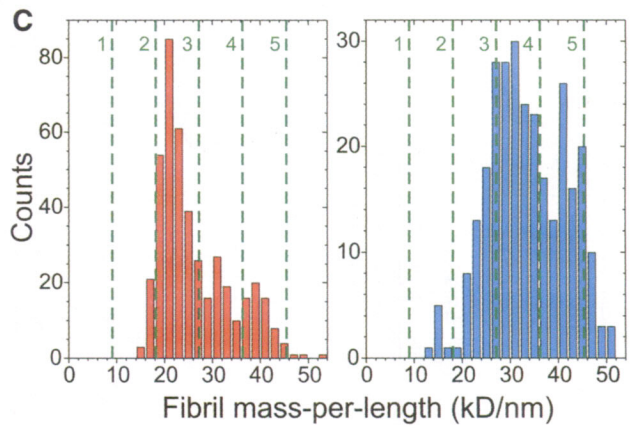

Fig. 4. Molecular structural features of quiescent (blue) and agitated (red) $A\beta_{1-40}$ fibrils. (**A**) Measurements of intermolecular ^{13}C-^{13}C nuclear magnetic dipole-dipole couplings for V12 carbonyl, A30 methyl, and V39 carbonyl carbons (circles, triangles, and squares, respectively) and numerical simulations for the indicated ^{13}C-^{13}C distances. Data were obtained for singly ^{13}C-labeled samples with the constant-time, finite-pulse, radio frequency–driven recoupling solid-state NMR technique (*9*, *14*). (**B**) Measurements of ^{15}N-^{13}C dipole-dipole couplings for D23 C_γ/K28 N_ζ and E22 C_δ/K16 N_ζ pairs (triangles and circles, respectively) and numerical simulations for the indicated ^{15}N-^{13}C distances. Data were obtained for samples with uniformly ^{15}N- and ^{13}C-labeled residues with the frequency-selective rotational echo double resonance solid-state NMR technique (*9*, *32*). Error bars are calculated from the root mean square noise in the NMR spectra. (**C**) MPL histograms extracted from STEM images of $A\beta_{1-40}$ fibrils. Dashed lines indicate MPL values for ideal cross-β structures with between one and five layers of $A\beta_{1-40}$ molecules. a.u., arbitrary units.

Reproduced with permission of the copyright owner. Further reproduction prohibited without permission.

molecular structure of the $A\beta_{1-40}$ protofilament (*13*, *15*). STEM, ^{15}N-^{13}C coupling, and chemical shift data for quiescent $A\beta_{1-40}$ fibrils indicate a qualitatively different structure in both molecular conformation and supramolecular organization. The largest chemical shift differences, suggesting the largest conformational differences, occur at Q15 and in residues 22 to 28. Although all residues in agitated $A\beta_{1-40}$ fibril samples exhibit one major set of ^{13}C chemical shifts (with the exception of D23, V24, and K28, possibly indicating the coexistence of two distinct D23-K28 salt bridge geometries), many residues in quiescent fibril samples exhibit two sets of ^{13}C chemical shifts, with an approximate 2:1 ratio of NMR signal intensities (e.g., I31 side-chain signals in Fig. 2). This observation raises the possibility that the quiescent $A\beta_{1-40}$ protofilament contains two structurally equivalent and one structurally inequivalent subunits, consistent with Fig. 4, B and C.

We point out four physical and biological implications of these data. First, the sensitivity of fibril morphology and molecular structure to growth conditions shows that at least two distinct fibril nucleation mechanisms exist for $A\beta_{1-40}$. One mechanism, leading to quiescent fibrils, may be purely homogeneous. The other mechanism, leading to agitated fibrils, may depend on the interface between the peptide solution and the air or the walls of the sample tube. The molecular structure of $A\beta_{1-40}$ fibrils is not determined solely by amino acid sequence and is not purely under thermodynamic control. Second, the phenomenon of strains in prion diseases, in which a single prion protein gives rise to multiple, distinct phenotypes, has been attributed to an ability of both mammalian and yeast prion proteins to adopt multiple, distinct amyloid-like structures. Observed differences in proteolysis patterns (*22*, *23*), resistance to chemical denaturation (*24*), seeding efficiencies (*25*), and electron paramagnetic resonance signals (*26*) support this proposal, but clear connections between morphological variations and molecular-level structural variations, between strains and morphological variations, and between strains and specific features of molecular structure have not yet been established experimentally. The correlations of amyloid fibril morphology with specific structural features established by our data, the demonstration of their self-propagating nature, and the observation of different neurotoxicities for different morphologies further strengthen the case for a structural origin of prion strains. Third, the importance of mature amyloid fibrils as etiological agents in AD and other amyloid diseases, as opposed to nonfibrillar oligomers observed at earlier stages of peptide incubation (*27–30*), is a subject of current controversy. One principal argument against a primary role for mature fibrils in AD has been the absence of a robust correlation between the severity of neurological impairment and the extent of amyloid deposition (*2*, *31*). Data in Fig. 3 raise the possibility that certain amyloid morphologies may be more pathogenic than others in the affected organs of amyloid diseases, which would weaken the correlation between disease symptoms and total amyloid deposition. Fourth, amyloid fibrils may prove useful as structural and chemical templates for self-assembled, one-dimensional nanomaterials with novel electronic or optical properties (*4*, *5*). Because structural uniformity is a likely prerequisite in such applications, the self-propagation of molecular structure demonstrated above may be important for reliable fabrication of amyloid-based nanomaterials.

References and Notes

1. M. Sunde, C. C. Blake, *Q. Rev. Biophys.* **31**, 1 (1998).
2. B. Caughey, P. T. Lansbury, *Annu. Rev. Neurosci.* **26**, 267 (2003).
3. R. Tycko, *Curr. Opin. Struct. Biol.* **14**, 96 (2004).
4. T. Scheibel *et al.*, *Proc. Natl. Acad. Sci. U.S.A.* **100**, 4527 (2003).
5. M. Reches, E. Gazit, *Science* **300**, 625 (2003).
6. C. S. Goldsbury *et al.*, *J. Struct. Biol.* **130**, 217 (2000).
7. J. L. Jimenez *et al.*, *Proc. Natl. Acad. Sci. U.S.A.* **99**, 9196 (2002).
8. J. D. Harper, S. S. Wong, C. M. Lieber, P. T. Lansbury, *Chem. Biol.* **4**, 119 (1997).
9. Materials and methods are available as supporting material on *Science* Online.
10. Single-letter abbreviations for the amino acid residues are as follows: A, Ala; C, Cys; D, Asp; E, Glu; F, Phe; G, Gly; H, His; I, Ile; K, Lys; L, Leu; M, Met; N, Asn; P, Pro; Q, Gln; R, Arg; S, Ser; T, Thr; V, Val; W, Trp; and Y, Tyr.
11. P. T. Lansbury *et al.*, *Nature Struct. Biol.* **2**, 990 (1995).
12. T. S. Burkoth *et al.*, *J. Am. Chem. Soc.* **122**, 7883 (2000).
13. A. T. Petkova *et al.*, *Proc. Natl. Acad. Sci. U.S.A.* **99**, 16742 (2002).
14. J. J. Balbach *et al.*, *Biophys. J.* **83**, 1205 (2002).
15. O. N. Antzutkin, R. D. Leapman, J. J. Balbach, R. Tycko, *Biochemistry* **41**, 15436 (2002).
16. C. P. Jaroniec *et al.*, *Proc. Natl. Acad. Sci. U.S.A.* **101**, 711 (2004).
17. D. S. Wishart, D. A. Case, *Methods Enzymol.* **338**, 3 (2001).
18. G. Cornilescu, F. Delaglio, A. Bax, *J. Biomol. NMR* **13**, 289 (1999).
19. M. Torok *et al.*, *J. Biol. Chem.* **277**, 40810 (2002).
20. I. Kheterpal, A. Williams, C. Murphy, B. Bledsoe, R. Wetzel, *Biochemistry* **40**, 11757 (2001).
21. A. D. Williams *et al.*, *J. Mol. Biol.* **335**, 833 (2004).
22. R. A. Bessen, R. F. Marsh, *J. Virol.* **66**, 2096 (1992).
23. G. C. Telling *et al.*, *Science* **274**, 2079 (1996).
24. J. Safar *et al.*, *Nature Med.* **4**, 1157 (1998).
25. P. Chien, J. S. Weissman, *Nature* **410**, 223 (2001).
26. M. Tanaka, P. Chien, N. Naber, R. Cooke, J. S. Weissman, *Nature* **428**, 323 (2004).
27. R. Kayed *et al.*, *Science* **300**, 486 (2003).
28. G. Bitan *et al.*, *Proc. Natl. Acad. Sci. U.S.A.* **100**, 330 (2003).
29. H. A. Lashuel, D. Hartley, B. M. Petre, T. Walz, P. T. Lansbury, *Nature* **418**, 291 (2002).
30. M. Bucciantini *et al.*, *Nature* **416**, 507 (2002).
31. M. D. Kirkitadze, G. Bitan, D. B. Teplow, *J. Neurosci. Res.* **69**, 567 (2002).
32. C. P. Jaroniec, B. A. Tounge, J. Herzfeld, R. G. Griffin, *J. Am. Chem. Soc.* **123**, 3507 (2001).

Supporting Online Material
www.sciencemag.org/cgi/content/full/307/5707/262/DC1
Materials and Methods
Figs. S1 to S4
Tables S1 and S2

15 April 2004; accepted 16 November 2004
10.1126/science.1105850

Semaphorin 3E and Plexin-D1 Control Vascular Pattern Independently of Neuropilins

Chenghua Gu,[1,2]* Yutaka Yoshida,[3]* Jean Livet,[4] Dorothy V. Reimert,[1,2] Fanny Mann,[4] Janna Merte,[1,2] Christopher E. Henderson,[4] Thomas M. Jessell,[3] Alex L. Kolodkin,[1]† David D. Ginty[1,2]†

The development of a patterned vasculature is essential for normal organogenesis. We found that signaling by semaphorin 3E (Sema3E) and its receptor plexin-D1 controls endothelial cell positioning and the patterning of the developing vasculature in the mouse. Sema3E is highly expressed in developing somites, where it acts as a repulsive cue for plexin-D1–expressing endothelial cells of adjacent intersomitic vessels. Sema3E–plexin-D1 signaling did not require neuropilins, which were previously presumed to be obligate Sema3 coreceptors. Moreover, genetic ablation of Sema3E or plexin-D1 but not neuropilin-mediated Sema3 signaling disrupted vascular patterning. These findings reveal an unexpected semaphorin signaling pathway and define a mechanism for controlling vascular patterning.

The peripheral nervous system and its vasculature develop coordinately in part through common developmental cues. Semaphorins, a family of phylogenetically conserved cell-surface and secreted proteins, control neuronal cell migration and axon guidance (*1–3*). Certain membrane-bound semaphorins bind directly to receptors of the plexin family (*4–7*), but the class 3 secreted semaphorins (Sema3A to Sema3F, referred to collective-

Reproduced with permission of the copyright owner. Further reproduction prohibited without permission.